Experiment and Theoretical Study of the Propagation of High Power Microwave Pulse in Air Breakdown Environment

Technical Semi-annual Report for the Work
Supported by AFGL through
NASA Grant No. NAG 5-1051

S.P. Kuo
Principal Investigator

A. Ren
Y.S. Zhang

April 12, 1990

Frequency Up-Conversion for the Reflectionless Propagation of a High-Power Microwave Pulse in a Self-Generated Plasma

S.P.Kuo, A.Ren and Y.S.Zhang
Weber Research Institute, Polytechnic University
Route 110, Farmingdale, NY 11735 USA

ABSTRACT

In the study of the propagation of high power microwave pulse, one of the main concerns is how to minimize the energy loss of the pulse before reaching the destination. In the very high power region, one has to prevent the cutoff reflection caused by the excessive ionization in the background air. A frequency auto-conversion process which can lead to reflectionless propagation of powerful EM pulses in self-generated plasmas is studied. The theory shows that under the proper condition the carrier frequency ω of the pulse will indeed shift upward with the growth of plasma frequency ω_{pe}. Thus, the plasma during breakdown will always remain transparent to the pulse (i.e., $\omega > \omega_{pe}$).

A chamber experiment to demonstrating the frequency auto-conversion during the pulse propagation through the self-generated plasma is then conducted in a chamber. The detected frequency shift is compared with the theoretical result calculated by using the measured electron density distribution along the propagation path of the pulse. Good agreement between the theory and the experiment results is obtained.

1. INTRODUCTION

In the applications of high power microwave pulses for radar and directed energy system, the effect of air breakdown on the propagation of the pulses through the atmosphere has been a central issue of research interest [1-7] This is because air breakdown produces ionization phenomena that can radically modify wave propagation. Moreover, a phenomenon called 'tail erosion' plays a primary role in limiting the transmission of pulse energy [6] Thus, a considerable effort for such a study has been pursued over the past decade. Both fluid and kinetic transport codes have been developed to give a self-consistent description of the propagation process. Many laboratory experiments have also been conducted to verify the results of computer codes.

The phenomenon of tail erosion can be described as follows. During the air breakdown, a space-time dependent plasma is generated. Considering any point along the path of the pulse, the plasma density is building up while the pulse is passing by. Since it takes finite time for the plasma to build up, the leading edge of the pulse can only have chance to interact with very few plasma electrons and is hardly affected. However, the plasma density at that point grows exponentially as the pulse continues passing by. By the time as the tail portion of the pulse is about to pass that point, a dense plasma is already present and can then attenuate this portion of the pulse significantly. The degree of tail erosion usually increases with the intensity of the pulse. By examining the dependence of

reflection signal on the degree of tail erosion in the transmission signal, two mechanism responsible for the tail erosion phenomenon have been identified experimentally in our previous work[6]. The first one is the collisional damping by the pulse-generated underdense plasma. It is shown that erosion to the tail of the pulse by this mechanism is not complete and there is no anomalous reflection. The loss of pulse's energy in this case may still be within the tolerable level. The second one is the cutoff reflection caused by the pulse-generated overdense plasma screen. In this case the incident pulse has higher intensity than that of the previous case and anomalous reflection is detected. The result shows that a large portion of the pulse is more or less eroded away during the finite propagation period. It is clear that the second mechanism is far more severe in causing energy loss of the pulse than the first one. Once the reflection mechanism is in play, the remaining pulse becomes too narrow to deliver enough energy as desired.

Obviously, one simple way to avoid cutoff reflection is to restrict the power of the pulse for a given pulse length to be lower than a critical power level. Unfortunately, this critical level is usually too low for the applications of interest. Therefore, it becomes essential to explore means for achieving reflectionless propagation of more powerful electromagnetic pulses through the atmosphere. Resently, Gildenburg et. al.[8] have point out that it is indeed possible to achieve reflectionless propagation of powerful EM pulses in an ionizing medium. Their analytical results show that a frequency auto-conversion process is in play in a nonstationary plasma. The carrier frequency ω of the pulse always shifts upward with the growth of plasma frequency ω_{pe} under the condition that the ionization frequency of the background air is much large than the collision frequency of electrons. Therefore, the plasma during breakdown will always remain transparent to the pulse (i.e., $\omega > \omega_{pe}$). Chamber experiments have also been conducted recently to demonstrate the frequency auto-conversion phenomenon[9,10]. The experimental results show that if the pulse is not distorted seriously (i.e., keeping $\omega > \omega_{pe}$) at the incident boundary, the pulse will not be distorted seriously and will experience frequency up-shift while ionizing the air during the subsequent period of propagation through the experimental chamber.

In this paper, a comprehensive theoretical and experimental study of the frequency auto-conversion process is reported. Presented in section II is a set of governing equations forming the basis of the theoretical model for describing pulse propagation in an ionizing air. The equation giving an explicit description of the frequency auto-conversion process is also derived and discussed. The pulse propagation experiments and the results are presented in section III. A comparison between the experimental results and the theory is made in section IV in which a discussion of the work is also given.

2. PROPAGATION OF A POWERFUL EM PULSE IN AN IONIZING AIR

The wave equation governing the propagation of an EM pulse in an ionizing medium is derived to be :

$$\{\frac{\partial^2}{\partial t^2} - c^2\frac{\partial^2}{\partial z^2} + \omega_{pe}^2[1 - i\nu/(\omega + i\bar{\nu})]\}E(z,t) = 0 \qquad (1)$$

where the electron momentum equation has been used to determine the current density induced by the wave field in the plasma; ν is the electron-neutral collision frequency, $\bar{\nu}=\nu+\nu_i$, and ν_i is the ionization frequency.

Since the plasma is generated by the pulse, its density (in terms of ω_{pe}^2) is a space-time function and is strongly dependent on the intensity and length of the pulse and on the loss processes including attachment, recombination and diffusion. When the power level of the pulse in consideration far exceeds the breakdown threshold of the air, however, the ionization rate ν_i of the air dominates over all the loss rates of the induced plasma. Thus, the rate equation for ω_{pe}^2 during the pulse period can be simplified to be :

$$\frac{\partial}{\partial t}\omega_{pe}^2 = \nu_i \omega_{pe}^2 \qquad (2)$$

where $\omega_{pe}^2 = 4\pi n_e e^2/m_e$ and the ionization frequency ν_i is modeled to be[11]

$$\nu_i = 3.83 \times 10^2 \nu_a [\varepsilon^{3/2} + 3.94\, \varepsilon^{1/2}]\exp[-7.546/\varepsilon] \qquad (3)$$

in which $\varepsilon = |E/E_{th}|$ is the wave field normalized to the breakdown threshold field E_{th} and ν_a is the attachment rate.

Equation (1) is analyzed by setting $E(z,t)=A(z,t)e^{-i\phi(z,t)}$, where the amplitude function $A(z,t)$ varies in space and time much slower than the phase function $\phi(z,t)$. This assumption is justifiable for a pulse containing many oscillations. Hence, $|\partial \ln A/\partial t| \ll |\partial\phi/\partial t|$ and $|\partial \ln A/\partial z| \ll |\partial\phi/\partial z|$. Using these approximations and the definition of local frequency $\omega=\partial\phi/\partial t$ and wavenumber $k=-\partial\phi/\partial z$, (1) is reduced to

$$\frac{\partial(\omega A^2)}{\partial t} + \frac{\partial(kc^2A^2)}{\partial z} = -\omega_{pe}^2 \nu\, \omega\, A^2/(\omega^2+\bar{\nu}^2) \qquad (4)$$

and

$$\omega^2 - k^2c^2 = \omega_{pe}^2[1 - \nu\bar{\nu}/(\omega^2+\bar{\nu}^2)] \qquad (5)$$

Equation (4) is the continuity equation for the energy density of the pulse, while (5) is the local dispersion relation. From the definition of ω and k, it requires that

$$\frac{\partial\omega}{\partial z} + \frac{\partial k}{\partial t} = 0 \qquad (6)$$

Equations (2)-(6) form a complete set of system equations describing the propagation of a one dimensional pulse in a self-generated plasma. To single out the frequency auto-conversion process, its governing equation is derived by taking the partial time derivative of (5) and using the relation (6) to simplify the result, the resulting equation is

$$\frac{\partial \omega^2}{\partial t} + v_g \frac{\partial \omega^2}{\partial z} = \{[1-\nu\bar{\nu}/(\omega^2+\bar{\nu}^2)]/[1-\omega_{pe}^2\nu\bar{\nu}/(\omega^2+\bar{\nu}^2)^2]\}\frac{\partial}{\partial t}\omega_{pe}^2 \qquad (7)$$

where $v_g = \partial\omega/\partial k$ is the group velocity of the pulse.

Under the conditions that $\nu\bar{\nu} \ll (\omega^2+\bar{\nu}^2)$ and $\omega_{pe}^2 \ll (\omega^2+\bar{\nu}^2)$, (7) is reduced to the one derived by Gildenburg et. al.[8]

$$\frac{d}{dt}(\omega^2 - \omega_{pe}^2) = -v_g \frac{\partial}{\partial z}\omega_{pe}^2 \qquad (8)$$

where $\frac{d}{dt} = \frac{\partial}{\partial t} + v_g\frac{\partial}{\partial z}$ is the total time derivative along the group trajectory of the pulse.

We now consider an example which is used to illustrate the physical implication of 8). Considering a rectangular pulse as shown in Fig. 1, the density of the generated plasma t a given time is expected to grow near exponentially from the background level at the ading edge of the pulse to a peak value at the tailend of the pulse. Behind the pulse, lasma density drops from the peak value at a rate depending on the loss mechanisms. he likely density profile is also plotted in Fig. 1. It is shown that $d\omega_{pe}^2/dz<0$ in the pulse terval and, consequently, $d(\omega^2-\omega_{pe}^2)/dt>0$. It, thus, leads to the conclusion that the plasma ill remain transparent (i.e., $\omega_{pe} < \omega$) to the pulse as long as $\omega > \omega_{pe}$ at the incident oundary. This conclusion seems trivial for a rectangular pulse propagating in a uniform medium in which $d\omega_{pe}^2/dt<0$. However, it becomes a significant result for pulse propagation in a nonuniform medium in which $d\omega_{pe}^2/dt>0$ can occur. An example of this ase is the propagation of a pulse through the atmosphere. Since the air pressure from the ground to the space decreases with the altitude, the breakdown threshold of air also decreases with the altitude before reaching an altitude having Paschen breakdown minimum. Beyond that altitude, the breakdown threshold increases with the altitude[5]. Thus, if the pulse is transmitted from the ground to the space, ω_{pe}^2 may increase ontinuously along the trajectory of the pulse and exceed $\omega_0^2=\omega^2(t=0,z=0)$ before reaching e altitude of Paschen minimum. However, there is no cutoff reflection throughout the ropagation, if $\omega > \omega_{pe}$ at the incident boundary. This is because ω is also continuously hifted upward through a frequency upconversion process. One can rewrite (8) to be $d\omega^2/dt = \nu_i\omega_{pe}^2 \geq 0$, it explains why ω also increases along the trajectory of the pulse. It is oted that such a frequency auto-conversion process is also applicable for pulse propagation from space to the ground since the altitude of the Paschen breakdown minimum is located in between.

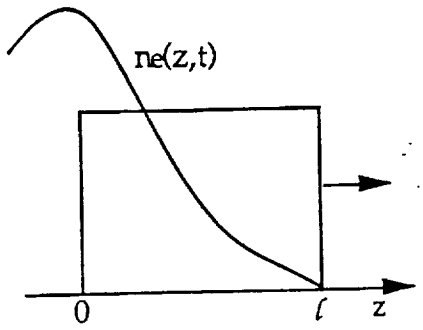

Fig.1 Envelope of a rectangular pulse and the pulse-generated electron density distribution.

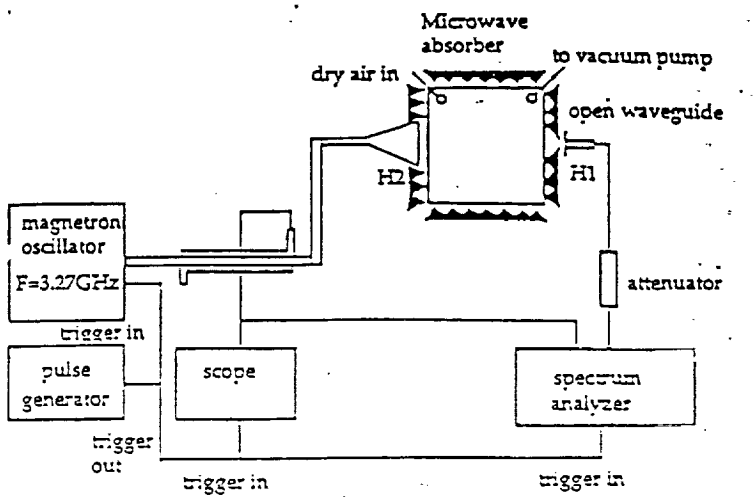

Fig.2 Experimental setup.

3. EXPERIMENTS

The experiment of pulse propagation is conducted in a vacuum chamber filled with dry air. The chamber is made of a 2 foot cube of Plexiglass. Microwave pulse is fed into the cube through a S-band microwave horn placed at one side of the chamber. A second S-band horn placed at the opposite side of the chamber is used to receive the transmitted pulse. The spectra of the incident pulse and transmitted pulse are then compared. The microwave power is generated by a single magnetron tube (OKH 1448) driven by a soft tube modulator. The magnetron produces 1MW peak output power at a central frequency of 3.27 GHz. The modulator uses a pulse forming network (PFN) having a pulse width of 1 μs and a repetition rate of 60 HZ.

The block diagram of the experimental setup is shown in Fig.2. A directional coupler connected to the incident horn is used to monitor the spectrum of the input pulse which is used as the reference. The air pressure in the chamber is about 0.08 torr, and thus, the electron-neutral collision frequency ν is below $5\times10^8 sec^{-1}$. Limited by the available power of the magnetron tube, the ionization frequency ν_i in such a background pressure is less than $10^8 sec^{-1}$. Hence, $\nu\bar{\nu} \ll \omega^2$. We also limit the power level of the input pulse so that the plasma density near the incident boundary is below the cutoff density, i.e. $\omega_{pe}^2(z=0) \le (\omega^2+\bar{\nu}^2)$. The assumptions used to reduce (7) to (8) are then justifiable with the present experiment.

The generated plasma density along the path of the pulse is measured in terms of the enhanced airglow whose relationship with the actual plasma density is calibrated by a Langmuir double probe. Using a focusing lens to localize the enhanced airglow, its temporal evolution at a fixed point is then recorded on the oscilloscope through a

photomultiplier tube. By moving the optical probe parallel to the path of the pulse, the variation of the peak airglow intensity along the path of the pulse is determined. It is noted that the airglow is generated mainly through impact excitation of neutral gas, which requires that electron energy exceeds 2eV . Hence, the axial distribution of the peak airglow intensity does not really represent, in general, the axial distribution of the peak plasma density. Nevertheless, it provides a good approximation especially since only the distribution of the peak airglow intensity is involved. Then the absolute value of the plasma density can be calibrated by measuring the plasma density with a Langmuir double probe at a point where the airglow intensity is also recorded simultaneously.

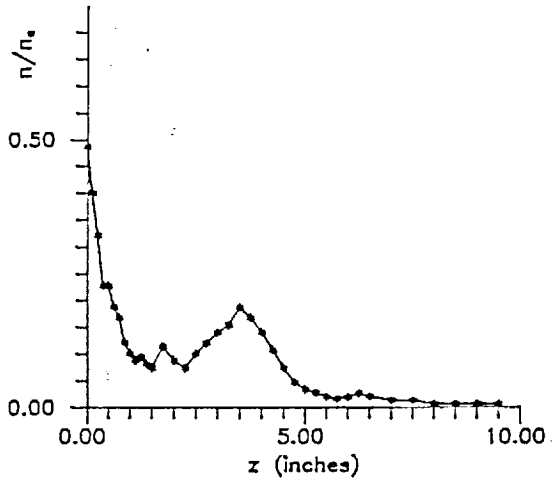

(a) Plasma density distribution with input power $P_1 \sim 1.1P_{th}$.

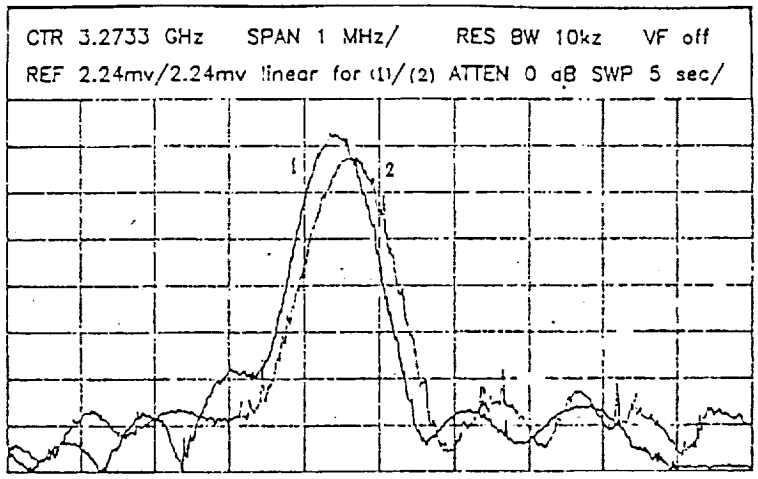

(b) Frequency spectra of the input (curve 1) and output (curve 2) pulses.

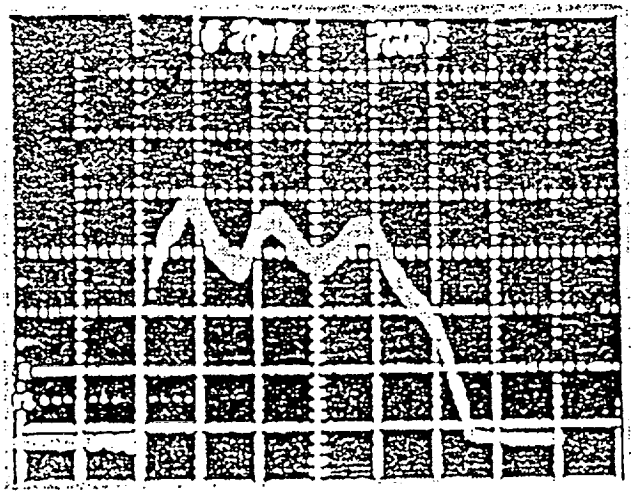

(c) The envelope of the input pulse.

Fig.3

We now compare the frequency spectrum of the input and output pulse for two different incident power levels, $P_1 \sim 1.1P_{th}$ and $P_2 \sim 1.46P_{th}$. Although the differences of these two levels seem not so significant, the results turn out quite different because the ionization rate is extremely sensitive to the field intensity. The corresponding density distribution along the propagation path and the envelope of the input pulse for each case is also measured for comparison. In the first case, $P_1 \sim 1.1P_{th}$, the peak density distribution of the generated plasma is shown in Fig.3a, which shows that the plasma density in this case is peaked at the incident boundary and decays quickly. The second peak is probably caused by the reflection of the chamber wall at the exit side. Excluding this peak, the density distribution appears to have a similar feature as the predicted one presented in Fig.1. Correspondingly, the induced frequency shift as shown in Fig. 3b. Presented in Fig. 3c is the envelope of the input pulse. In Fig. 3b, curve 1 is the frequency spectrum of the input pulse, while curve 2 is the frequency spectrum of the output pulse. The frequency difference between the peaks of these two curves represents the frequency shift attributed to the plasma generation in the chamber. The power level $P_2 \sim 1.46P_{th}$ in the second case is chosen for achieving the maximum frequency shift without sacrificing the distortion of the pulse. The set of frequency spectra for the input pulse (curve 1) and output pulse (curve 2) is presented in Fig.4b. As shown in Fig. 4a, the plasma density in this case is much higher than that of the previous case shown in Fig. 3a.

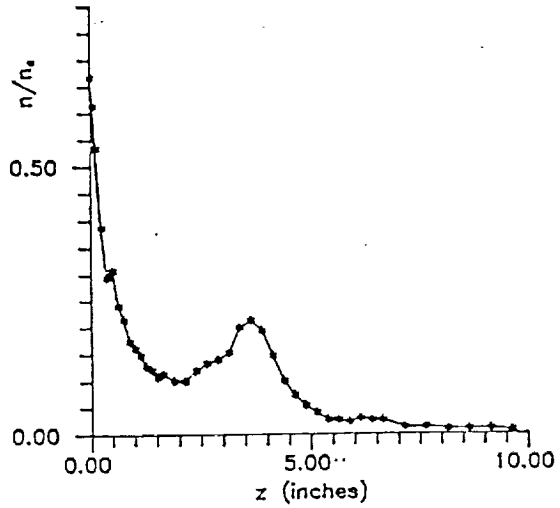

(a) Plasma density distribution with input power $P_2 \sim 1.46P_{th}$.

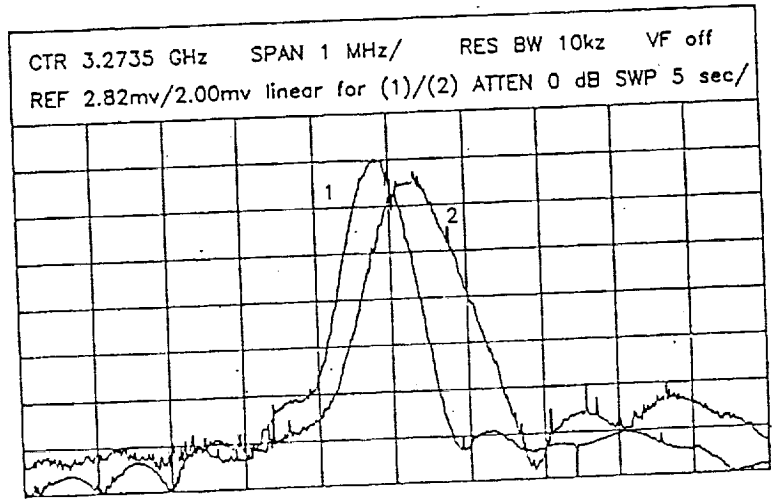

(b) Frequency spectra of the input (curve 1) and output (curve 2) pulses.

Fig.4

4. COMPARISON AND DISCUSSION

With the aid of (2) and the definition of $\frac{d}{dt}$, (8) can be reduced to

$$\frac{d}{dt}\omega^2 = \nu_i\omega_{pe}^2 \tag{9}$$

It is integrated to obtain the frequency shift

$$\Delta f \cong (f_0/2c)\int_0^L dz\, \nu_i(n/n_c)/(1-n/n_c)^{1/2} \tag{10}$$

where $dt = dz/v_g \sim dz/[c(1-n/n_c)^{1/2}]$ and $\nu^2 << \omega_0^2 = \omega^2(0)$ are assumed; L is the length of the chamber.

Therefore, Δf can be evaluated once n(z) and $\nu_i(z)$ are specified. Since the length of the chamber ~ 0.6m is much shorter than the pulse's spatial length ~300m, the spatial variation of ν_i will be neglected in the following calculation. Moreover, if the input pulse is approximated by a rectangular pulse having a constant amplitude E_0 and a pulse length τ, $\nu_i=\nu_i(E_0)$ during the pulse duration is approximately calculated from the relation $\nu_i=\ln(n/n_0)/\tau$, where $n_0=n(z,t=0)$ is the initial background electron density in the chamber. Thus (10) reduces to

$$\Delta f \sim [f_0/2c\tau]\int_0^L dz\, (n/n_c)\ln(n/n_0)/(1-n/n_c)^{1/2} \tag{11}$$

We now use the density distribution displayed in Figs 3a and 4a to carry out the integration of (11). The corresponding results are obtained to be Δf_1=0.27Mhz and Δf_2=0.40Mhz. From Figs 3b and 4b, the frequency shifts are measured for the two corresponding cases to be Δf_1=0.300Mhz and Δf_2=0.426Mhz, respectively. A good agreement between the theoretical and the experimental results is clearly shown.

In this work, a frequency auto-conversion process for a powerful microwave pulse propagating in a self-generated plasma is studied. The theory is first presented and the equation explaining the frequency auto-conversion process is derived. This equation indicates that if $\omega > \omega_{pe}$ at the incident boundary, and the depletion of the pulse energy by the self-generated plasma is small, then ω increases along the propagation path of the pulse and is always larger than ω_{pe} throughout the propagation. A pulse propagation experiment for confirming the theoretical prediction of frequency auto-conversion phenomenon is conducted. The frequency spectra of the input and output pulses are recorded simultaneously for comparison. The corresponding peak density distribution along the propagation path of the pulse is also determined through the measurement of airglow enhancement by an optical probe. Using the measured density distributions, the corresponding frequency shifts for two incident pulses of different amplitudes are evaluated. They are then compared with the experimental results. A good agreement is found.

The frequency auto-conversion process enables a high power electromagnetic pulse to propagate through an inhomogeneous medium, such as the atmosphere, whose

breakdown minimum is located between the incidence boundary and the destination. This process is thus expected to make the operation of the high power radar and directed energy system easier and more effective.

5. ACKNOWLEDGEMENT

This work was supported by the Air Force system command, Air Force Office of Scientific Research Grant No. AFOSR-91-0002 and by the Air Force Geophysical Laboratory through NASA Grant No. NAG 5-1051.

6. REFERENCES

1. W.M. Bollen, C.L. Yee, A.W. Ali, M.J. Nagurney, and M.E. Read, J.Appl. Phys. 54, 101 (1983); C.L. Yee, A.W Ali, and W.M.Bollen, J. Appl. Phys. 54, 1278(1983).

2. Wee Woo and J.S. DeGroot, Phys. Fluids. 27, 475(1984).

3. J.H. Yee, R.A. Alverez, D.J. Mayhall, D.P. Byrne, and J.DeGroot, Phys. Fluids. 29, 1238 (1986).

4. M.J.Mulbrandon, J.Chen, P.J.Palmadesso, C.A.Sullivan, and A.M.Ali , Phys. Fluids B.1, 2507 (1989).

5. S.P. Kuo and Y.S.Zhang, Phys. Fluids B, 2, 667 (1990)

6. S.P. Kuo , Y.S. Zhang, and Paul Kossey, J. Appl. Phys. 67, 2762 (1990).

7. S.P. Kuo, Y.S. Zhang, P. Kossey, and R.J.Barker, NATO AGARD Conf. Proc., in press.

8. V.B. Gildenburg, V.A. Krupnov, and V.E. Semenov, Pis'ma V. Zh. Teh. Fiz. 14, 1695 (1988).

9. S.P. Kuo, Phys. Rev. Lett. 65(8), 1000(1990).

10. S.P. Kuo, Y.S. Zhang, and A. Ren, Phys. Lett. A 150(2), 92(1990).

11. Yu.A.Lupan, Sov. Phys. Tech. Phys. 21(11), 1367(1976).

Simulation of intense microwave pulse propagation in air breakdown environment

S.P. Kuo and Y.S. Zhang
Weber Research Institute
Polytechnic University
Farmingdale, NY 11735

ABSTRACT

An experiment is conducted to examine the tail erosion phenomenon which occurs to an intense microwave pulse propagating in air breakdown environment. In the experiment, a 1 MW microwave pulse (1.1μs) is transmitted through a large plexiglas chamber filled with dry air at about 1~2 torr pressure. Two different degrees of tail erosion caused by two different mechanisms are identified. This experimental effort leads to the understanding of the fundamental behavior of tail erosion and provides a data base for validating the theoretical model.

A theoretical model based on two coupled partial differential equations is established to describe the propagation of an intense microwave pulse in air breakdown environment. One is derived from the Poynting theorem, and the other one is the rate equation of electron density. A semi-empirical formula of the ionization frequency is adopted for this model. A transformation of these two equations to local time frame of reference is introduced so that they can be solved numerically with considerably reduced computation time. This model is tested by using it to perform the computer simulation of the experiment. The numerical results are shown to agree well with the experimental results.

1. INTRODUCTION

When a high power microwave pulse propagated through a region of the atmosphere where the breakdown threshold field of the background air is lower than the field intensity of the pulse, the ionization is expected to occur and produces a space-time dependent plasma. Such a plasma can attenuate the pulse and gives rise to a phenomenon called tail erosion which plays the primary role in limiting the transmission of the pulse energy.[1-4] Moreover, the propagation characteristics of the pulse can also be radically modified by the nonlinear and nonlocal effects of the self-generated space-time dependent plasma.[4,5] Therefore, any meaningful theoretical effort on the study of pulse propagation through the atmosphere requires a self-consistent description of the propagation process and a justification with available experimental results.[6,7]

Basically, there are two fundamental issues to be addressed. The first one concerns the optimum pulse characteristics for maximum pulse energy transfer through the atmosphere. The second concern is maximizing the ionizations in the plasma trail following the pulse for providing sufficient focusing to compensate for wave spreading. In general, these two concerns are interrelated and must be considered together. This is because the density of the plasma providing the focusing effect depends on the intensity of the pulse. On the other hand, the loss of the pulse's intensity may cause excessive ionization in one region where the overdense plasma can cut off the propagation of a large portion of the pulse. Once reflection occurs, the remaining pulse will become too narrow for effective ionization during the remaining journey. The more serious matter is that the remaining pulse will be too narrow to carry enough energy as desired.

In this research effort, a pulse propagation experiment is first conducted in a chamber to demonstrate the tail erosion phenomenon. A theoretical model describing the propagation of an intense microwave pulse in air breakdown environment is then developed. We next use the theoretical model to simulate the experiment whose results, in turn, are used to validate the model. This model can then be used to simulate the more general cases and determine the conditions avoiding the occurrence of cutoff reflection.

The pulse propagation experiment and results are presented in Section 2. The modal equations describing pulse propagation are presented in Section 3. In Section 4, a numerical analysis simulating the experiment is made. A frame transformation to convert the modal equations into a local time domain description is introduced in Section 5. The resultant equations are shown more readily for describing long distance propagation because much less computing time is required. The new set of modal equations is normalized according to the relevant parameters of the atmosphere and is ready for the numerical analysis of an EM pulse propagating through the atmosphere. This work is summarized and discussed in Section 6.

2. EXPERIMENTS

Experiments are conducted in a chamber made of plexiglass filled with dry air at about 1 torr pressure.[3] A microwave pulse is fed into the cube by an S-band microwave horn placed at one side of the chamber. A second S-band horn placed at the opposite side of the chamber is used to receive the transmitted pulse. The chamber is shielded with microwave absorbers so that the microwave reflection from the walls and nearby structures can be minimized. Shown in Fig. 1 is the block diagram of the experimental setup.

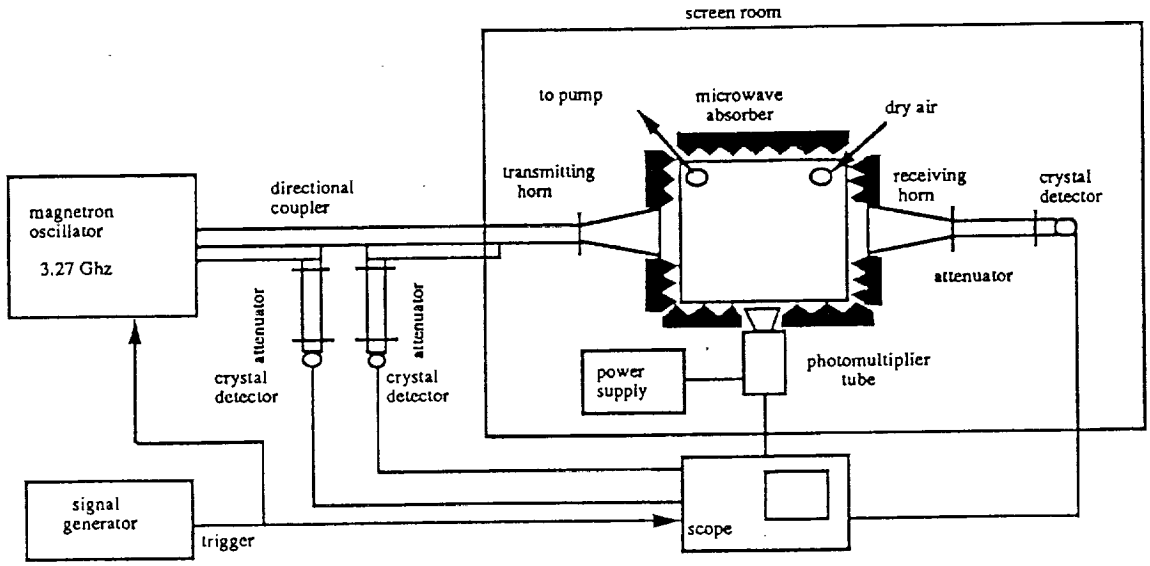

Figure 1. Experimental setup of high power microwave pulse propagation

Tail erosion is a common phenomenon appearing in the propagation of a high power microwave pulse (HMP). This phenomenon is demonstrated by the snapshots presented in Fig. 2, where 1.1μs pulses, with four consecutively increasing amplitudes, are transmitted through the chamber. The first one has a field amplitude below the breakdown threshold field of the background air so nothing happens. Consequently, the received pulse shape as shown in Fig. 2(a) is undistorted from that of the input pulse. However, once the field amplitude of the input pulse exceeds the breakdown threshold, tail erosion occurs and becomes more serious to the larger amplitude pulses, as is shown by the subsequent snapshots (Figs. 2(b)-2(d)). This is understandable because the strong increase of the ionization rate with field amplitude allows more electrons, which attenuate the pulse,to build up. The last two snapshots (Figs. 2(c) and 2(d)), show that the pulses have been strongly eroded. However, a clear distinction between the fundamental behavior of tail erosion in the two cases is also

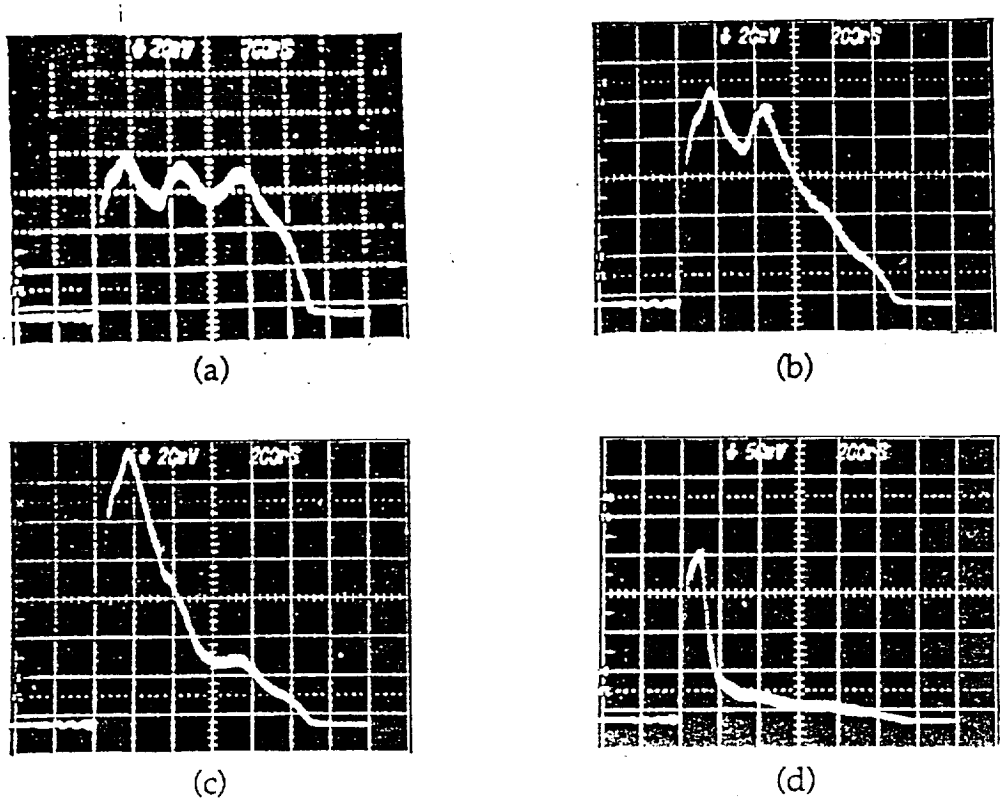

Figure 2. Tail erosion of microwave pulses of four consecutively increasing amplitudes

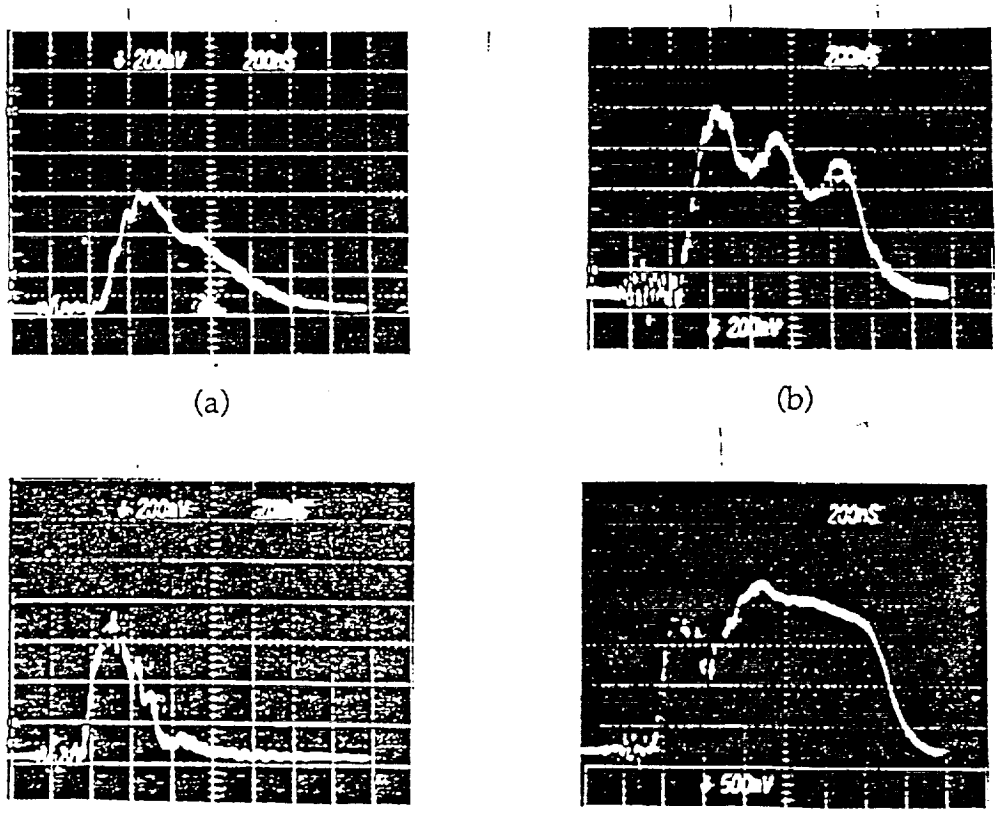

Figure 3. received pulses and coresponding reflected pulses

noticed. In one case corresponding to the third picture (Fig. 2(c)), the erosion to the tail of the pulse is not complete. In other words, the received pulse width extends to the original width. In the other case (Fig. 2(d)), a large portion of the pulse is more or less eroded completely during the finite propagation period. Obviously, it is a different mechanism responsible for the second case. The ionization frequency becomes so large in the second case that the electron density exceeds the cutoff density of the wave before the whole pulse passes through the chamber. The overdense plasma screen reflects the remaining portion of the pulse and causes even more severe tail erosion. In order to verify that the tail erosion in the second case is indeed caused by cutoff reflection, the reflected power for each case is also measured for comparison. Each of the two snapshots (Figs. 3(b) or 3(d)) presented on the RHS of Fig. 3 is the envelope of the reflected pulse corresponding to each received pulse presented on its left (Figs. 3(a) or 3(c)). The second set of snapshots (Figs. 3(c) and 3(d)) shows that strong reflection and complete erosion appear together. In conclusion, two mechanisms responsible for the tail erosion are identified. One is due to attenuation by the self-generated underdense plasma. The other one is caused through reflection by the self-generated overdense plasma screen.

Our experimental results (Figs. 3(a) and 3(c)) clearly demonstrate that an increase of pulse amplitude may not help to increase the energy transfer by the pulse. This is because two tail erosion mechanisms have different impacts on causing the degradation of the pulse energy transfer. Once cutoff reflection is allowed to happen, the additional energy added to the pulse is practically wasted by the reflection. The practical way to solve this problem is either lowering the amplitude of the pulse or narrowing the pulse width so that the excessive ionization can be avoided. It is, therefore, essential to determine the optimum parameters of the pulse for achieving the most effective energy transfer and ionization. Because the effect of pressure gradient and large propagation distance cannot be incorporated in the chamber experiment, these parameters can be determined via the numerical simulation based on a proposed theoretical model which, however, has to be validated first by the available experimental data.

3. THEORETICAL MODEL

The Poynting theorem is used to describe the energy flow of the high power wave propagation in air breakdown environment, it leads to the equation

$$\nabla \cdot \frac{c}{4\pi} (\vec{E} \times \vec{B}) + \frac{\partial}{\partial t} (E^2 + B^2)/8\pi = -\vec{J} \cdot \vec{E} \tag{1}$$

where $\vec{J}$ is the wave-induced current density in the self-generated plasma.

The self-generated plasma is described by the rate equation for the electron density

$$\frac{\partial n}{\partial t} = (\nu_i - \nu_a) n - \gamma n^2 \tag{2}$$

together with the momentum equation of electrons

$$\frac{\partial}{\partial t} \vec{V} = -\frac{e\vec{E}}{m} - (\nu + \nu_i)\vec{V} = -\frac{e\vec{E}}{m} - \nu_1 \vec{V} \tag{3}$$

where γ is the recombination coefficient, ν, ν_i, and ν_a are collision frequency, ionization frequency, and attachment frequency, respectively, and $\nu_1 = \nu + \nu_i$.

In the present study, a one-dimensional model of wave propagation under forward scattering approximation is considered. We express the wavefield and the velocity response of the electrons as

$$\vec{E} = \frac{1}{2} \vec{E}_0 e^{-i\omega t} + \text{c.c.} \quad \text{and} \quad \vec{V} = \frac{1}{2} \vec{V}_0 e^{-i\omega t} + \text{c.c.} \tag{4}$$

where $\vec{E}_0$ and $\vec{V}_0$ are the vector phase amplitudes and functions of z and t.

Substituting (4) into (3), yields

$$\vec{V}_0 = -\frac{e}{m}\left(\nu_1 + \frac{\partial}{\partial t} - i\omega\right)^{-1} \vec{E}_0 \tag{5}$$

Thus, the induced current density is derived to be

$$\vec{J} = -en\vec{V} = e^{-i\omega t}\,\frac{ne^2}{2m}\,\frac{\left(\nu_1+\frac{\partial}{\partial t}+i\omega\right)}{\left(\nu_1+\frac{\partial}{\partial t}\right)^2+\omega^2}\,\vec{E}_0 + \text{c.c.}$$

$$\approx e^{-i\omega t}\,\frac{\omega_p^2}{8\pi(\omega^2+\nu_1^2)}\left(\nu_1 + \frac{\partial}{\partial t} + i\omega\right)\vec{E}_0 + \text{c.c.} \tag{6}$$

where we have neglected $\frac{\partial}{\partial t}$ terms in the denominator of (6) for a slowly time varying function E_0, i.e., $\left|\frac{\partial}{\partial t}\ln E_0\right| \ll \omega$.

Taking time average of $\vec{J}\cdot\vec{E}$ over one period of the wave carrier, yields

$$\langle \vec{J}\cdot\vec{E} \rangle = \frac{\omega_p^2}{8\pi(\omega^2+\nu_1^2)}\left(\nu_1 + \frac{1}{2}\frac{\partial}{\partial t}\right)E_0^2 \tag{7}$$

The time average of (1) then becomes

$$\frac{\partial}{\partial z}\,\frac{c}{8\pi}\,E_0B_0 + \frac{\partial}{\partial t}\,\frac{1}{16\pi}\left[B_0^2 + \left(1 + \frac{\omega_p^2}{\omega^2+\nu_1^2}\right)E_0^2\right]$$

$$= -\frac{\nu_1\omega_p^2}{8\pi(\omega^2+\nu_1^2)}\,E_0^2 \tag{8}$$

where the forward scattering approximation is used to simplify the resultant equation. This approximation is used because we are only interested in the energy transfer in the forward direction and is justifiable because the density distribution of the induced plasma is, in general, smooth enough for neglecting the effect of multiple scattering.

Introducing the notations

$$P = \frac{1}{16\pi}\left[B_0^2 + \left(1 + \frac{\omega_p^2}{\omega^2+\nu_1^2}\right)E_0^2\right] \equiv \frac{1}{8\pi}\,E_0^2 \tag{9}$$

and

$$S = \frac{c}{8\pi}\,E_0B_0 \equiv \frac{c}{8\pi}\,E_0^2\left[1 - \omega_p^2/(\omega^2+\nu_1^2)\right]^{1/2} = v_gP \tag{10}$$

where P and S are the energy density and power flux of the wave respectively, and $v_g = c[1-\omega_p^2/(\omega^2+\nu_1^2)]^{1/2}$ is the (group) velocity of the energy flow.

Equation (1) is finally reduced to:

$$\frac{\partial P}{\partial t} + \frac{\partial}{\partial z}(v_g P) = -\beta P \tag{11}$$

where $\beta = \nu_1 \omega_p^2/(\omega^2 + \nu_1^2)$.

Equation (11) is coupled with Eq. (2) through the ionization frequency ν_i, which is given by[9]

$$\nu_i/\mathcal{P} = 2.5\times10^7[8.8(\overline{P})^{1/4} + 2.236(\overline{P})^{3/4}] \exp(-7.546/\overline{P}^{1/2}) \text{ (sec-torr)}^{-1} \tag{12}$$

where $\mathcal{P}$ is the background pressure in torr; $\overline{P} = P/P_{cr}$, $P_{cr} = E_{cr}^2/8\pi$, and $E_{cr} = 36.84p(1+\omega^2/\nu^2)^{1/2}$ V/cm is the breakdown threshold field of the background air of pressure p. These two equations, together with (12) give a self-consistent description of pulse propagation in an air breakdown environment.

4. COMPUTER SIMULATION

Introducing the dimensionless variables and functions: $\overline{n} = n/n_c$, $\overline{P} = P/P_{cr}$, $\tau = \sqrt{\nu_a \nu}\, t$, $z' = \sqrt{\nu_a \nu}\, z/c$, $\overline{v_g} = (1-\overline{n})^{1/2}$, and $\overline{\beta} = (\nu_1/\sqrt{\nu_a \nu})\overline{n}$, where $n_c = (m/4\pi e^2)(\omega^2 + \nu_1^2)$, (2), (11) and (12) are normalized to be

$$\frac{\partial \overline{n}}{\partial \tau} = (\nu_a/\nu)^{1/2} A \overline{n} \tag{13}$$

$$\frac{\partial \overline{P}}{\partial \tau} + \frac{\partial}{\partial z'}(\overline{v_g}\,\overline{P}) = -\overline{\beta}\,\overline{P} \tag{14}$$

and

$$A = \nu_i/\nu_a - 1 = 3.83\times10^2[\overline{P}^{3/4} + 3.94\overline{P}^{1/4}] \exp[-7.546/\overline{P}^{1/2}] - 1 \tag{15}$$

where the recombination loss term in (2) is neglected and the attachment frequency $\nu_a = 6\times10^4 p \text{ sec}^{-1}$ is measured by the Bragg scattering method.[8]

We now model the envelope of the normalized energy density of the incident pulses employed in the chamber experiments to be

$$\overline{P}_0 = \overline{P}(\tau, 0) = \alpha \exp[-(\tau/\tau_0)^{10}] \tag{16}$$

where $\tau_0 \approx \sqrt{\nu \nu_a}\, t_0/2$ is the normalized pulse width; t_0 is the pulse width and set equal to 1-1μs in this simulation.

To solve (13) and (14) numerically, we used a software package developed by Richard F. Sincovec and Nile K. Madsen[10] for nonlinear partial differential equations. This package is an interface routine which uses centered difference approximations to convert one dimensional systems of partial differential equations of the form

$$\frac{\partial \vec{u}}{\partial t} = F\left(t, x, \vec{u}, \frac{\partial \vec{u}}{\partial x}, \frac{\partial^2 \vec{u}}{\partial x^2}\right) \tag{17}$$

into an explicit system of first order differential equations of the form

$$\frac{\partial \vec{u}}{\partial t} = G(t, x, \vec{u}) \tag{18}$$

Then it utilizes the widely used ODE integrator subroutine[11] to solve these partial differential equations by calculating the time derivatives of the functions at mesh points from neighboring spatial points and integrating in time domain to get the solution. This program is written in FORTRAN and can be run on Cray in the Pittsburgh Super Computing Center.

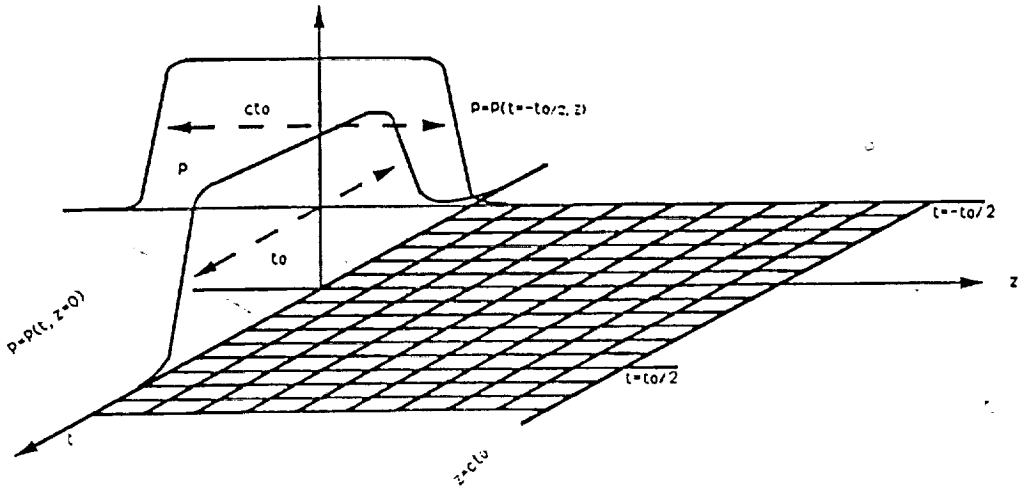

Figure 4. Boundary and initial condition of the simulation

The boundary condition and initial condition for the pulse's energy density are best shown in Fig. 4. The initial condition of electron density is $\overline{n}=\overline{n}_0$ for all z; and the density at the boundary will be determined from $\overline{P}(t,z=0)$ with the restriction of $\overline{n}\leq 1$. The differential equations are solved in a two dimensional surface determined by $z=z'$ and $t=\tau$ axes. The number of the mesh points are chosen so as to minimize the numerical error. For the results shown here, we have $N_m=1000$, $N_t=1000$.

Shown in Fig. 5 are four different degrees of tail erosion on four different incident pulses $\alpha_1=1$, $\alpha_2=3.5$, $\alpha_3=5$, $\alpha_4=9$ propagating over the chamber length (x=66 cm), where the vertical axis represents the pulse's amplitude ($A_i=P_i^{1/2}$). Comparing these plots with those presented in Fig. 2 of the corresponding experimental results, good agreement is found.

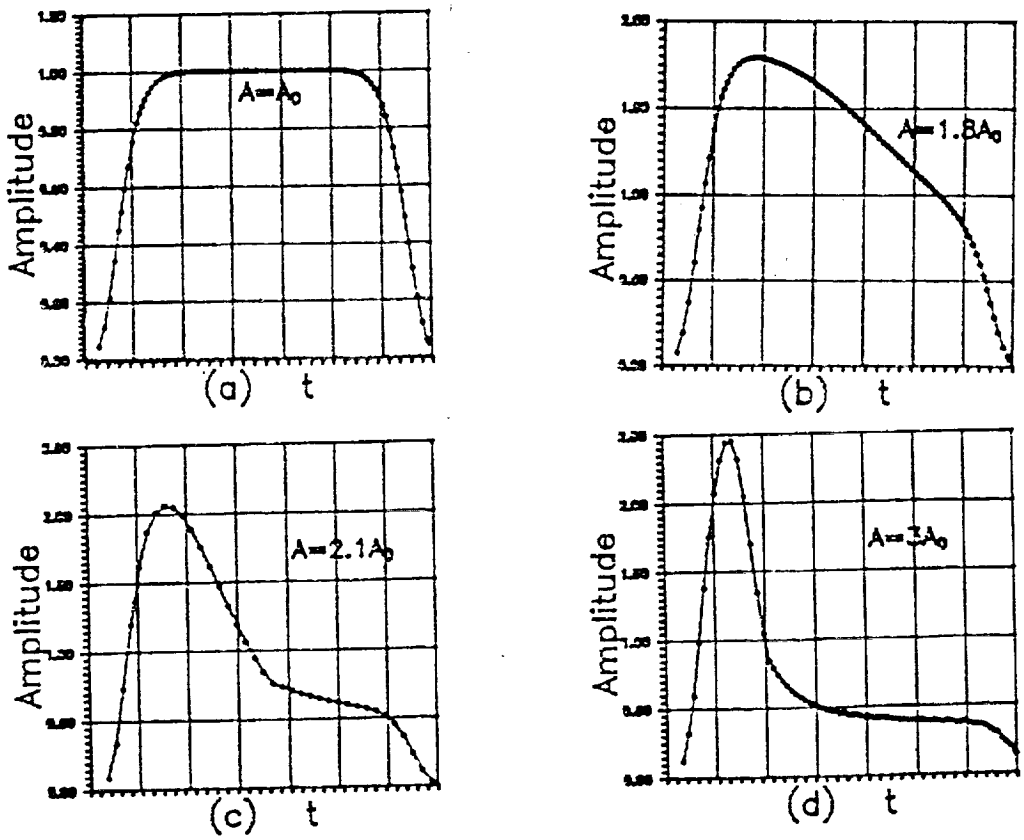

Figure 5. Tail erosion of 1.1μs microwave pulses for four consecutive increasing amplitudes (computer simulation)

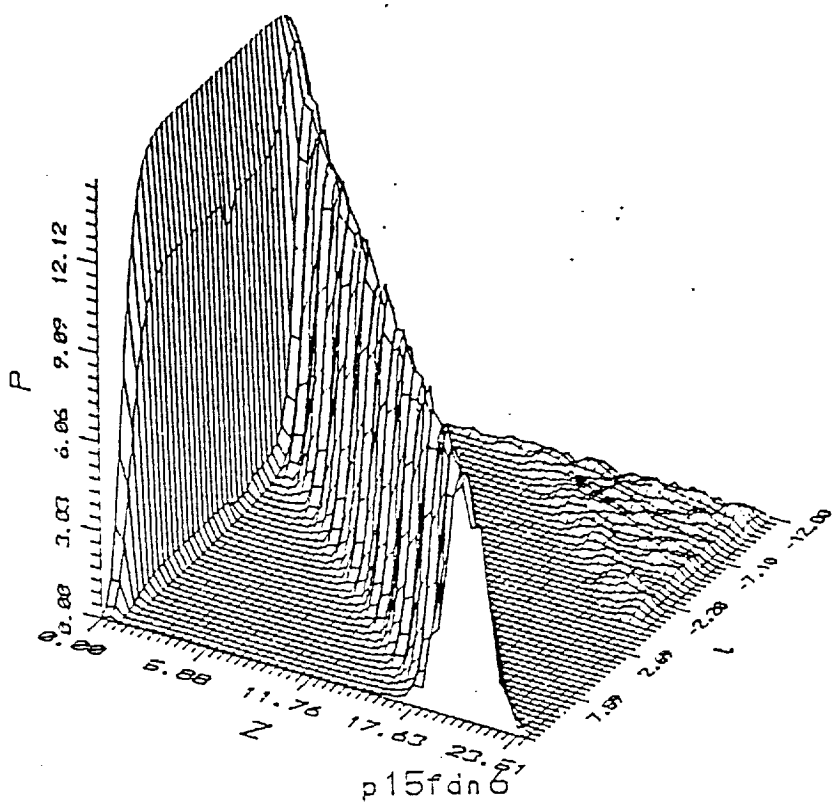

Figure 6. (a) Microwave pulse envelop as a function of time and space

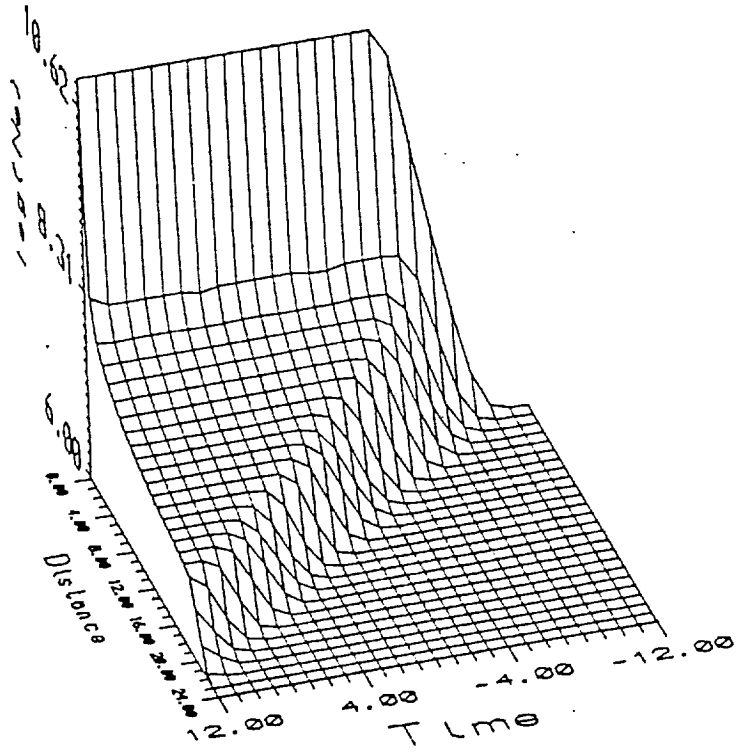

Figure 6. (b) Electron density as a function of time and space

The numerical results (Fig. 5) of tail erosion phenomenon also reveal two distinctive features similar to the experimental observations. For instance, the pulse envelope presented in Fig. 5(b) shows a linear decay starting from the front portion of the pulse. In constrast, the pulse envelope presented in Fig. 5(d) shows a sharp drop in the amplitude rather than a gradual decay. These features confirm with the experimental results shown in Fig. 3, where two received microwave pulses with the abovementioned two different features of tail erosion are recorded (Figs. 3(a) and 3(c)).

The good agreement between the numerical simulation and the experimental results suggests that Eqs. (2) and (11) together with (12) represent a very good theoretical model for describing high power microwave pulse propagation in air breakdown environment. Thus, the numerical solutions of these two modal equations can provide information about the spatial variations of the pulse energy and electron density which are not easy to be measured experimentally.

Shown in Figs. 6(a) and 6(b) are the three dimension drawings of pulse amplitude and electron density versus space and time for the case of pulse amplitude $\alpha = 15$, and the initial electron density $n_o = 10^6 cm^{-3}$. It shows that the electron density will rise very rapidly at the boundary to reach the cutoff density $\overline{n} = 1$, and thus to form a high density thin layer. This high density electron layer will absorb and reflect the remaining portion of the pulse. Therefore, only the leading edge of the pulse, about one-fifth of the initial pulse width, passes through the high density layer and propagates continuously in the forward direction. The transmitted pulse now have lower amplitude and much narrower width than those of the incident pulse, the generated electron density, hence, drops sharply after the thin layer and maintains a relative constant level following the trail of the pulse.

5. FRAME TRANSFORMATION OF THE MODAL EQUATIONS

In validating the theoretical model by the experimental results, one has only to integrate numerically the modal equations (2) and (11) over the chamber distance which is relatively short, and thus, the computation time does not appear to be a problem. However, in the practical applications of pulse propagation over a large distance, the required computation time becomes an important issue. Apprarently, the cause of consuming large computation time comes from the simultaneous appearance of space and time derivatives in Eq. (11). One common way to eliminate such a problem is to use a frame transformation to convert (2) and (11) into a local time domain description. In doing so, the space and time derivatives can be separated from the same equation, and the computation time on the resultant equations for the same propagation distance can be saved tremendously.

Since the group velocity v_g of the pulse is a space and time function, the frame transformation is defined to be

$$t = t' + \int_0^{z'} dz''/V_g(t',z'') \qquad (19)$$

and

$$z = z'$$

where t' is the local time of the pulse and $V_g(t',z') = v_g(t,z)$. Thus, the partial differential operators in the two frames are related by

$$\partial/\partial t = f(t',z')\partial/\partial t'$$

and

$$\partial/\partial z = \partial/\partial z' - [f(t',z')/V_g(t',z')]\,\partial/\partial t'$$

where $f(t',z') = [1 - \int_0^{z'} dz''(V_{gt'}/V_g^2)]^{-1}$ and $V_{gt'} = \partial V_g/\partial t' \cong -(c^2/2V_g n_c)(\partial N/\partial t')$.

Equations (2) and (11) are then transformed to be

$$\frac{\partial}{\partial t'}N = [(\nu_i-\nu_a)N-\gamma N^2]/f \tag{21}$$

and

$$\frac{\partial}{\partial z'}V_g P_1 = -[\beta-(V_{gt'}/V_g)f]P_1 \tag{22}$$

where $N(t',z')=n(t,z)$ and $P_1(t',z')=P(t,z)$.

With the aid of (21) and (22), the integration in $f(t',z')$ can be carried out, and it leads to

$$\begin{aligned} f(t',z') &= \exp\{-\int_0^{z'} dz'' c^2[(\nu_1-\nu_a)N-\gamma N^2]/2V_g^3 n_c\} \\ &= (V_g P_1/V_{go}P_{10})\exp\{\nu_1 \int_0^{z''} dz'(N/n_c)/V_g\} \end{aligned} \tag{23}$$

where $V_{go}=V_g(t',z'=0)$ and $P_{10}=P_1(t',z'=0)$. Substituting (23) into (21) and (22), yields

$$\frac{\partial}{\partial t'}N = \nu_a AN(V_{go}P_{10}/V_g P_1)\exp\{-\nu_1 \int_0^{z'} dz''(N/n_c)/V_g\} \tag{24}$$

and

$$\frac{\partial}{\partial z'}V_g P_1 = -[\nu_1 + c^2\nu_a A/2V_g^2]P_1 N/n_c \tag{25}$$

where A is defined the same as (15) witih $\overline{P}=P_1/P_{cr}$; and $\nu_1=\nu+\nu_i$.

Equations (24) and (25) can be solved by using ODE software package directly for pulse propagation over a long distance. The required computation time will be much less than that needed for solving the original Eqs. (2) and (11) which need an additional interface routine converting (11) from the PDE or into an explicit ODE or before using the ODE integrator subroutine.

The main purpose of this study is to develop a useful model for numerical analysis of pulse propagation through the atmosphere. The feature of altitude dependence of the background pressure has to be included in the model. This, in turn, causes ν, ν_a, ν_i, P_{cr}, and n_c all become altitude dependent. Therefore, (24) and (25) cannot be normalized directly in terms of these parameters as made in Section 4. Instead, the parameter values at the location of 1 torr pressure (near the Paschen minimum) are chosen for the normalization purpose. We assume that the air pressure at 50 km height is 1 torr, and the pressure is an exponential decay function of the altitude z'. Thus, $p(z')=760e^{-1.33\times10^{-4}z'}$ torr, where z' is measured in meters. Let $\nu_o=\nu(z'=0)$, then $\nu=\nu_o e^{-1.33\times10^{-4}z'}$. In terms of the ground level dc breakdown threshold power $P_{co}=P_{cr}(z'=0,\omega=0)$, then $P_{cr}(z')=P_{co}(\eta+e^{-2.66\times10^{-4}z'})$, where $\eta=\omega^2/\nu_o^2$. Similarly, $n_c=n_{co}(\eta+e^{-2.66\times10^{-4}z'})$, where $n_{co}=m\nu_o^2/4\pi e^2$. At 1 torr pressure, $\nu_a=\nu_{ac}=6\times10^4\,\text{sec}^{-1}$ and $\nu=\nu_c=6\times10^9\,\text{sec}^{-1}$ for 1 eV electron temperature. Including the effect of electron energy change by the incident pulse and assuming that the unperturbed background temperature is about 0.01 eV, a modal function for ν is given by $\nu=\nu_c p[\overline{P}^{1/2}+0.01]^{1/2}$, where $\overline{P}=P/P_{cr}=(P/P_{co})\ (\eta+e^{-2.66\times10^{-4}z'})^{-1}$. We now introduce the dimensionless variables and functions as follows: $(\nu_c\nu_{ac})^{1/2}t'\rightarrow t$, $(\nu_c\nu_{ac})^{1/2}z'/c\rightarrow z$, $\overline{n}=N/n_c=(N/n_{co})h(z)\rightarrow n$, where $h(z)=(\eta+e^{-4.2\times10^{-5}z})^{-1}$, $P_1=P/P_{co}\rightarrow P_1$,

$Q=(1-\overline{n})^{1/2}\overline{P_1}\rightarrow(1-n)^{1/2}P_1$, $P_1=Q/(1-n)^{1/2}$, and $\overline{P}\rightarrow P_1h(z)=(Q/\sqrt{1-n})h(z)$. In terms of these dimensionless variables and functions, and notice that $(\nu_c/\nu_{ac})^{1/2}=316$ and $(\nu_c\nu_{ac})^{1/2}=1.9\times10^7\,sec^{-1}$. Equations (24), (25) and (15) become

$$\frac{\partial}{\partial t}n = 2.41g(z)An(Q_o/Q)\exp\{-2.4\times10^5\int_o^z f(x)dx\} \tag{26}$$

$$\frac{\partial}{\partial z}Q = -2.41g(z)\left\{(316)^2[(P_1h)^{1/2}+0.01] + \frac{1}{2}A/\sqrt{1-n}\right\}nQ/\sqrt{1-n} \tag{27}$$

and

$$A = 3.83\times10^2\{(P_1h)^{3/4} + 3.94(P_1h)^{1/4}\}\exp\{-7.546/(P_1h)^{1/2}\}-1 \tag{28}$$

where $g(z)=e^{-2.1\times10^{-3}z}$, $f(x)=g(x)\{[P_1(x)h(x)]^{1/2}+0.01]^{1/2}\,[n(x)/\sqrt{1-n(x)}\,]$ and $Q_o=Q(t,z=0)$.

Equations (26)-(28) are the set of modal equations describing microwave pulse propagation through the atmosphere either from ground to space or from space to ground. If the pulse is oblique propagation with an angle θ with respect to the vertical axis, what one has to do is to replace V_g by $V_g\cos\theta$, i.e., replacing $\sqrt{1-n}$ by $\sqrt{1-n\cos\theta}$ in (26) and (27), for a correct description. In terms of z and t, the real distance x and time τ are given by $x=15.8\,z(m)$ and $\tau=52.63\,t(ns)$.

6. SUMMARY AND DISCUSSION

The propagation of a high power microwave pulse through a self-generated plasma is studied. A chamber experiment is first conducted to explore the unique features appearing in the pulse as the result of the breakdown of the background air. The most apparent one is tail erosion. It demonstrates that air breakdown can indeed radically modify wave propagation and limit the energy transfer by the pulse. Two mechanisms responsible for two different degrees of tail erosion have been identified. The serious one happens when the initial intensity of the pulse is too high and causes complete erosion to a large tail portion of the pulse during the finite propagation. It is identified as a result of the reflection by the self-generated overdense plasma screen. It can be realized by the fact that the ionization frequency becomes too large, the electron density can build up quickly and exceed the cutoff density of the wave before the whole pulse passes through. The results show that once reflection occurs, the remaining pulse will become too narrow to deliver enough energy as desired. Therefore, there is a need to find the optimum pulse parameters for achieving maximum energy transfer. Consequently, a theoretical model developed for this purpose would be more practical. The experimental results of the present work are then used for validating the established theoretical model of high power microwave pulse propagation in the atmosphere.

The self-consistent description of the propagation process is provided by the set of two modal equations including Poynting's equation for the continuity of the power flux of the pulse and the rate equation of the electron density. A forward wave approximation model is used to simplify Poynting's equation and a semi-emperical formula for ν_i as a function of the field amplitude is used to express the electron rate equation explicitly. This set of modal equations is then used to simulate the chamber experiment. The numerical results are shown to agree very well with the experimental results, especially the unique features of two distinctive degrees of tail erosion identified from the experimental results can be reproduced by the numerical results of the modal equations. This comparison serves as a validation of the established theoretical model.

In order to improve the numerical efficiency of the model in terms of the required computation time and available subroutines for numerical analysis of pulse propagation over a long distance, a transformation to the frame of local time of the pulse is introduced. The effect of space-time dependence of the group velocity of the pulse is included in this properly designed transformation. The resultant equations are reduced to the forms which can be solved directly by the available subroutine of ODE solver. In terms of relevant parameters of the atmosphere, these two equations are normalized for numerical analysis of pulse propagation in the atmosphere. It is noted that the inhomogeneous feature of the background pressure is preserved in the model, thus, the model is capable for a description of long distance pulse propagation.

7. ACKNOWLEDGEMENT

This work was supported by the Air Force Geophysical Laboratory through NASA Grant No. NAG5-1051, and by the Air Force System Command, Air Force Office of Scientific Research, Grant No. AFOSR-91-0002. The numerical work was performed at the Pittsburgh Supercomputing Center which is supported by the National Science Foundation.

8. REFERENCES

1. W.M. Bollen, C.L. Yee, A.W. Ali, M.J. Nagurney and M.E. Read, J. Appl. Phys. 54, 101 (1983); C.L. Yee, A.W. Ali and W.M. Bollen, ibid, 54, 1278 (1983).
2. J.H. Yee, R.A. Alvarez, D.J. Mayhall, N.K. Madsen and H.S. Cabayan, J. Radiat. Eff. Res. Eng., 3, 152 (1984).
3. B. Goldstein and O.C. Longmire, J. Radiat. Eff. Res. Eng., 3, 1626 (1984).
4. S.P. Kuo, Y.S. Zhang and P. Kossey, J. Appl. Phys., 67, 2762 (1990).
5. W. Woo and J.S. DeGroot, Phys. Fluids, 27, 475 (1984).
6. J.H. Yee, R.A. Alvarez, D.J. Mayhall, D.P. Byrne and J. DeGroot, Phys. Fluids, 29, 1238 (1986).
7. M.J. Mulbrandon, J. Chen, P.J. Palmadesso, C.A. Sullivan and A.W. Ali, Phys. Fluids, B1, 2507 (1989).
8. S.P. Kuo and Y. S. Zhang, Phys. Fluids, B2, 667 (1990).
9. Y.A. Lupan, Sov. Phys. Tech. Phys., 21, 1367 (1976).
10. R.F. Sincovec and N.K. Madsen, ACM Trans. Math. Software, 1(3), (1975).
11. K.L. Herbert and L.F. Shampine, Sandia National Laboratories Report SAND80-0180 (1990).